Macromolecular Rapid Communications
www.mrc-journal.de

Fusion-Induced Growth of Biomimetic Polymersomes: Behavior of Poly(dimethylsiloxane)-Poly(ethylene oxide) Vesicles in Saline Solutions Under High Agitation

Nika Marušič, Ziliang Zhao, Lado Otrin, Rumiana Dimova, Ivan Ivanov, and Kai Sundmacher*

Giant unilamellar vesicles serve as membrane models and primitive mockups of natural cells. With respect to the latter use, amphiphilic polymers can be used to replace phospholipids in order to introduce certain favorable properties, ultimately allowing for the creation of truly synthetic cells. These new properties also enable the employment of new preparation procedures that are incompatible with the natural amphiphiles. Whereas the growth of lipid compartments to micrometer dimensions has been well established, growth of their synthetic analogs remains underexplored. Here, the influence of experimental parameters like salt type/concentration and magnitude of agitation on the fusion of nanometer-sized vesicles made of poly(dimethylsiloxane)-poly(ethylene oxide) graft copolymer (PDMS-*g*-PEO) is investigated in detail. To this end, dynamic light scattering, microscopy, and membrane mixing assays are employed, and the process at different time and length scales is analyzed. This optimized method is used as an easy tool to obtain giant vesicles, equipped with membrane and cytosolic biomachinery, in the presence of salts at physiological concentrations.

1. Introduction

The bottom-up approach within synthetic biology aims to reproduce the organization and functions of living cells by their stepwise assembly.[1] This inherent reductionism will eventually allow elucidating the fundamental principles of life but also transferring them to man-made systems that could serve as life mimics. A far goal of the above process is the reconstitution of self-reproduction, where one of the prerequisites is membrane formation and expansion, as postulated in the simplistic framework of chemotons.[2] A significant progress has been recently seen on the biosynthetic side of prokaryotic scenarios, including an eight-enzyme cascade and liposome growth[3] or genetic programming and feedback regulation of cell-free systems within liposomes.[4] Looking at eukaryotes though, we confront the yet unclear mechanism of phospholipid (i.e., membrane) transport from the lipid factory to the target organelle. In fact, the understanding of this complex phenomenon is very limited compared to protein trafficking. Even though the contribution of secretory pathways[5] cannot be easily ruled out, non-vesicular transport via contacts and appositions seems to emerge as predominant mechanism.[6] However, disrupting the contacts between endoplasmic reticulum and plasma membrane in yeast did not affect sterol transport and suggested protein shuttling instead.[7] In any case, vesicle fusion has been nearly the only rewarding method to observe visible growth of liposomes with natural chemistry,[8] and next to proteins, has been induced by physicochemical triggers like charge[9] or osmotic tension.[10] Moreover, regardless of the precise biological blueprint and context, the uptake of preformed membrane building blocks is conceptually equivalent to the uptake of membrane precursors and thus represents a valid synthetic approach.

Synthetic chemistry allows for significant broadening of the properties of cytomimetic compartments by using the same self-assembly principles.[11] Polymer vesicles have been initially acclaimed with respect to their toughness[12] compared to liposomes, while biological compatibility, relevance and practical merits are continuously being introduced. For instance, polymers increased the functional lifetime of respiratory proteins[13]

N. Marušič, L. Otrin, I. Ivanov, K. Sundmacher
Process Systems Engineering
Max Planck Institute for Dynamics of Complex Technical Systems
Sandtorstraße 1, 39106 Magdeburg, Germany
E-mail: ivanov@mpi-magdeburg.mpg.de
Z. Zhao, R. Dimova
Department of Theory and Bio-Systems
Max Planck Institute of Colloids and Interfaces
Science Park Golm
14424 Potsdam, Germany
Z. Zhao
Leibniz Institute of Photonic Technology e.V.
07745 Jena, Germany
Z. Zhao
Faculty of Physics and Astronomy
Institute of Applied Optics and Biophysics
Friedrich Schiller University Jena
07743 Jena, Germany

The ORCID identification number(s) for the author(s) of this article can be found under https://doi.org/10.1002/marc.202100712

DOI: 10.1002/marc.202100712

and their resistance to oxidative stress.[14] Furthermore, analogous to liposomes, polymersomes can be morphed to various shapes, including stomatocytes[15] and even undergo orchestrated fusion mediated by synaptic machinery.[16] Yet the fusion of polymersomes by simpler physicochemical cues is underexplored. One of the few existing examples reported fusing poly(trimethylene carbonate)-poly(L-glutamic acid) vesicles below the melting temperature of the hydrophobic block and ascribed it to conformational change and variation of membrane packing.[17] In this regard, freeze-thaw cycling of lipid protocells was also investigated as an environmental driver for exchange of nucleic acids.[18] In another example, fusion of poly(*N*-isopropylacrylamide)-*b*-poly(6-[4-(4-methylphenyl-azo) phenoxy] hexylacrylate) (PNIPAM-*b*-PAzoM) giant vesicles was observed, caused by the increased polarity of the isomerized azobenzene units on the hydrophobic block upon irradiation.[19] Meanwhile, ultrasound treatment induced fusion of polymersomes, generated from the molecular self-assembly of an amphiphilic multiarm copolymer with a hyperbranched poly(3-ethyl-3-oxetanemethanol) core and multiple poly(ethylene oxide) arms (HBPO-star-PEO).[20] Furthermore, polymerization-induced polymersome fusion and development of tubular polymersomes was achieved by exploiting the unique features of aqueous ring-opening metathesis polymerization-induced self-assembly (ROMPISA).[21] Finally, upon addition of PEO to poly(ethylene oxide)$_{16}$-*b*-poly(butylene oxide)$_{22}$ (EB1) polymersome dispersions, the latter aggregated and fused.[22] In parallel, large unilamellar vesicles (LUVs) of poly(ethylene oxide)-poly(butadiene) blocks (PBd-*b*-PEO) were shown to form giant vesicles upon agitation simply in presence of NaCl solutions.[23] We adopted this facile approach for the more biocompatible graft poly(dimethylsiloxane)-poly(ethylene oxide) (PDMS-*g*-PEO), which forms layers of similar thickness to lipid bilayers but is softer than most lipids and slightly less fluid,[14] and were able to form micrometer vesicles. To this end, we followed the effect of salt type and concentration next to the vortex magnitude by dynamic light scattering (DLS) and microscopy, and monitored membrane mixing via dye dequenching and fluorescence resonance energy transfer (FRET). To further investigate the process, we also added LUVs to the microcompartments via bulk mixing and in microfluidic traps. Finally, we checked the enzymatic activity of protein-functionalized polymersomes, subjected to the optimized fusion protocol, and exposed the growing PDMS-*g*-PEO polymersomes to several water-soluble compounds in order to study their encapsulation, retention, and interaction with the membrane.

2. Results and Discussion

2.1. Polymer Nanocompartments Grow to Microns

PDMS-*g*-PEO vesicles were prepared by extrusion through 200-nm pores, according to the reported protocol.[24] Via DLS, we tested the effect of $MgCl_2$ and KCl, next to NaCl that was previously used for fusion of PBd-*b*-PEO LUVs. No size change was observed in 5–250 mM divalent or monovalent salts upon incubation at room temperature for up to one week. Salts might destabilize the vesicle suspensions but even the highest concentrations did not induce polymersome aggregation (**Figure 1**A). The size did not change with agitation (0–1200 rpm) in Milli-Q water, sucrose or 5–50 mM salt solutions either. In contrast, 200 nm PBd-*b*-PEO polymersomes were shown to fuse in low salt concentration (10 mM NaCl) after 1 h at 20 Hz (1200 rpm).[23] Here, we observed the formation of larger PDMS-*g*-PEO vesicles only after 8 h agitation at 1200 rpm in 250 mM NaCl, as shown by the additional small peak at ≈5 μm (Figure 1B). Further agitation (24 h) resulted in more micron-sized structures, though another new peak at ≈30 nm reflected concomitant fission and/or lysis. Samples with $MgCl_2$ exhibited similar behavior but the two new populations appeared sooner (Figure 1C). In presence of 250 mM KCl though, the monodisperse polymersome suspension nearly doubled its size only after 3 h, and after 7–8 h the intensity of the ≈5 μm peak substantially increased (Figure 1D). Increasing the concentration of KCl to 350 mM did not improve the aggregation/fusion efficiency and neither did faster agitation at 1300 rpm. The latter merely caused the appearance of smaller vesicles (Figure 1E) as in the presence of $MgCl_2$, which effect was further substantiated at 1500 rpm due to the higher shear stress. Unlike salts, agitation at 1300 rpm in Milli-Q did not cause fission of polymersomes; their size remained unchanged even after 24 h vigorous vortexing (Figures S1–S3, Supporting Information). The influence of different salts and agitation speed is summarized in **Figure 2** and Table S1, Supporting Information.

As DLS cannot distinguish between aggregated and fused vesicles and suffers from a limited upper range, microscopy confirmed that the micrometer structures were giant unilamellar vesicles (GUVs); agitation at 1200 rpm for 3 h in 250 mM KCl resulted in GUVs with diameters of 4–20 μm and some of the polymersomes were clustered and closely apposed (Figures S4 and S5, Supporting Information). While cryo-TEM previously revealed that PDMS-*g*-PEO forms exclusively unilamellar vesicles under isotonic conditions,[14] agitation of PBd-*b*-PEO led to mixtures of uni- and multilamellar ones.[25] To increase the yield and potentially the size of the GUVs, we increased the initial concentration of polymer from 1.25 to 5 mg mL^{-1} and the time of agitation from 3 to 24 h. In addition, we facilitated the microscopic analysis by incorporation of tagged polymer (PDMS-*g*-PEO-Rhodamine) at 1.2 mol% loading. Indeed, the amount of GUVs substantially increased but the size did not exceed 25 μm (Figure S6, Supporting Information) and a smaller portion of the vesicles became multivesicular. With the same agitation, we did not find any vesicles larger than 1 μm in 250 mM NaCl and 125 mM $MgCl_2$.

The GUVs larger than 20 μm in diameter contained a lower amount of labeled polymer compared to the smaller ones, which corresponded to our previous observations on polymersomes, formed by partial dehydration of LUVs and electroformation.[14] Both occurrences suggest that the dye hampers fusion, which might be associated with steric or charge effects, even though the difference between the nearly neutral zeta potentials of labeled and non-labeled polymersomes was rather small in 250 mM KCl due to charge screening (Figure S8, Supporting Information). Since higher polymer loading improved the yield of GUVs, we further doubled the LUV amount to 10 mg mL^{-1} and reduced the amount of labeled amphiphile twice (to 0.6 mol%). Those two factors had a positive effect on the growth and GUVs with diameter of 40 μm could be found in the sample (Figure S7, Supporting Information).

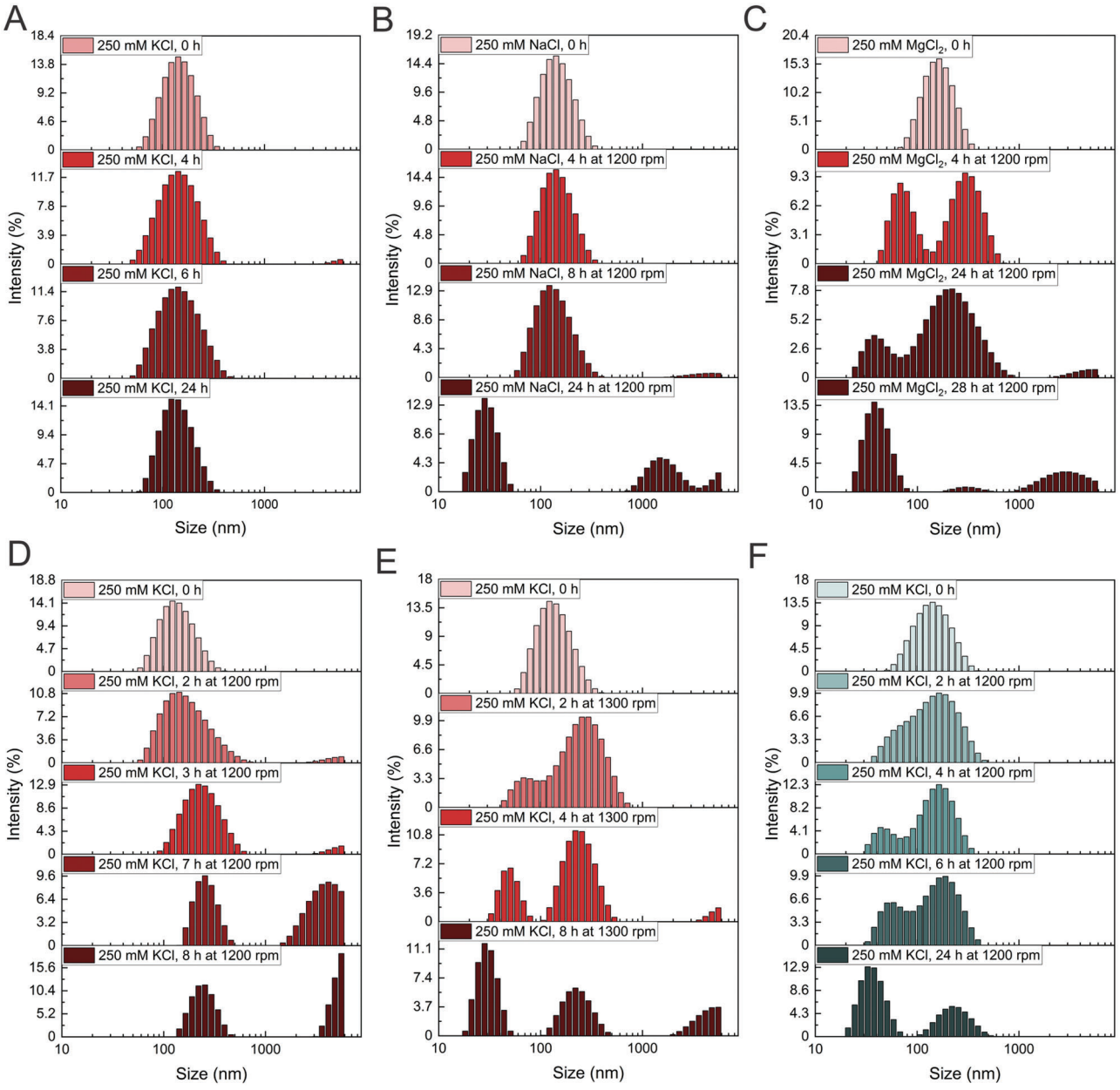

Figure 1. Time-resolved size distribution of vesicles (1.25 mg mL^{-1}) with salt and agitation. Salt-to-polymer molar ratio is 600:1 and the measurement volume is 400 µL. A) Polymersomes in 250 mM KCl in absence of agitation. B) Polymersomes in 250 mM NaCl agitated at 1200 rpm. C) Polymersomes in 250 mM $MgCl_2$ agitated at 1200 rpm. D) Polymersomes in 250 mM KCl agitated at 1200 rpm. E) Polymersomes in 250 mM KCl agitated at 1300 rpm. F) Hybrid vesicles in 250 mM KCl agitated at 1200 rpm. Hybrids size distribution in 250 mM KCl in absence of agitation can be found in Figure S9, Supporting Information.

Next, we benchmarked PDMS-*g*-PEO against natural lipids. No apparent change in the size distribution of DOPC liposomes was observed in 250 mM KCl at 1200 rpm. Furthermore, agitation of hybrid vesicles composed of 80 mol% PDMS-*g*-PEO and 20 mol% DOPC (an amphiphile ratio that ensures homogenous distribution[26]) caused only a decrease in vesicle size (Figure 1F). The mechanical stress apparently destabilized the hybrids, via either rupture/fission or phase separation and budding, thus the presence of lipids prevented fusion at the given conditions.

Finally, we induced membrane defects via hypotonic shocks since pores may act as nucleation sites for fusion, and also applied hypertonic conditions. Osmotic difference >150 mOsmol kg^{-1} was previously demonstrated to induce fusion of adjacent lipid membranes (vesicles in contact with a planar bilayer),[27] while on the other hand, rigid block polymersomes may explode when exposed to osmotic shock.[28] Neither hypertonic incubation nor hypotonic conditions in presence or absence of agitation changed the vesicle size (Figures S10 and S11, Supporting Information). We ascribed the intactness to the regulation of osmotic

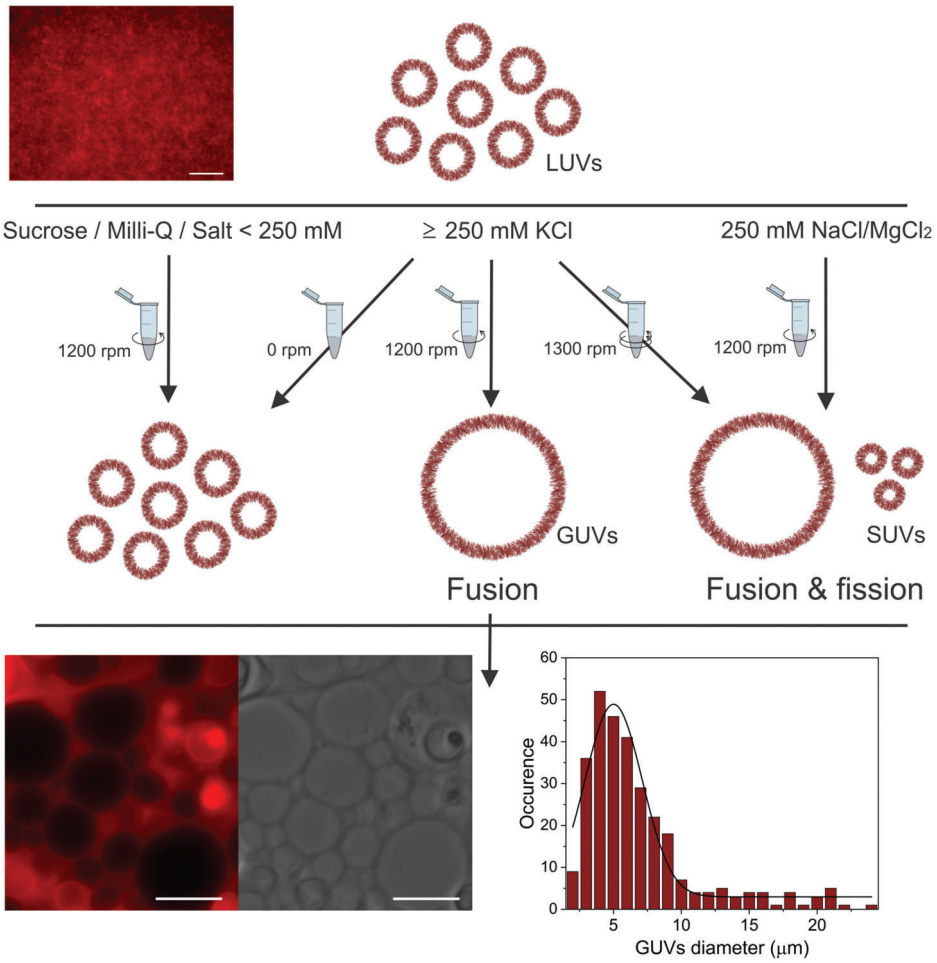

Figure 2. Scheme summarizing the influence of salts and agitation on PDMS-*g*-PEO polymersomes. Microscopy images (in epifluorescence and transmitted light mode) of samples of LUVs (5 mg mL^{-1}) in 250 mM KCl before agitation are shown in the upper micrograph, and the resulting GUVs after 24 h at 1200 rpm (in 1.5 mL Eppendorf tube) are shown in the lower one. Scale bars: 10 μm. Membrane was tagged with labeled polymer (1.2 mol% PDMS-*g*-PEO-Rhodamine). The right lower panel shows the respective size distribution of GUVs ($n = 300$).

stress by transient pore opening,[29] which released the membrane tension and counteracted fusion.

In all examples above, we investigated fusion and growth, starting from LUVs extruded by 200-nm filter. To test if extrusion can be circumvented, we also tried to grow GUVs from polymer film under the same conditions (250 mM KCl was added directly to a dried polymer film). After 24 h at 1200 rpm we obtained mixed population of LUVs and small GUVs (with diameters of 1–2 μm) (Figures S12 and S13, Supporting Information). This indicated that the optimal starting material for the current procedure is a population of relatively small LUVs. Apparently, increased positive membrane curvature accelerates the fusion process (previously demonstrated for charge-mediated liposome fusion[30]), which was likely the case for the present system too.

2.2. Membrane Mixing

When only a small portion of vesicles fuse, they may not be detected in DLS. Meanwhile, only micrometer-sized polymersomes can be optically accessed. Because of this, to further assess fusion, we monitored membrane mixing via the dequenching of a hydrophobic dye 1,1″-dioctadecyl-3,3,3″,3′-tetramethylindotricarbocyanine iodide (DiR), which was previously used for PBd-*b*-PEO vesicles,[31] and also measured the decreasing FRET signal between 7-nitrobenz-2-oxa-1,3-diazol-4-yl (NBD) and fluorescein (FITC) or lissamine rhodamine B sulfonyl (Rho). Membrane mixing of DiR-LUVs and dye-free LUVs results in dilution of the dye, which restores its fluorescence (Figure S14A, Supporting Information). Indeed, the intermittently measured DiR fluorescence increased with agitation at 1200 rpm and the continuous dequenching could be followed directly in the spectrophotometer cuvette (Figure S15, Supporting Information). Though, the newly formed micron-sized structures did not resemble the previously observed GUVs and appeared as polymer beads (Figure S16, Supporting Information). Similar structures were observed in populations of PEO_{16}-*b*-PBO_{22} vesicles upon addition of 20 kDa PEO.[22] Higher DiR concentrations have been also shown to promote the fusion of liposomes to cells for staining purposes[32] and the weak size control of DiR-DOPC liposomes[31] may be also related to similar interactions.

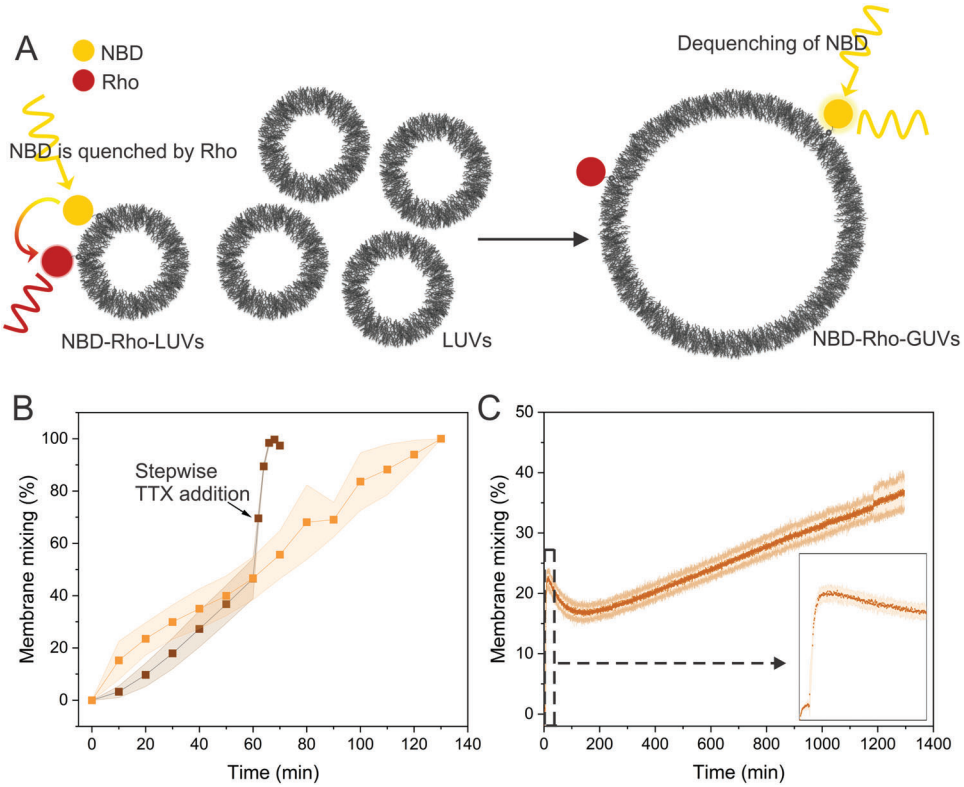

Figure 3. Membrane mixing via dilution of labeled lipids (PE-NBD and PE-Rho) and monitoring of NBD fluorescence (ex/em = 460/535 nm). A) Scheme representing the FRET setup. Tagged (1.5 mol% PE-Rho and PE-NBD) and bare polymersomes are mixed in volume ratio 1:4. Upon their fusion, NBD is dequenched and its fluorescence increases. B) Intermittent membrane mixing at 1200 rpm. Points represent the averages of four samples and shaded area shows the standard deviation. 100% FRET signal is obtained by lysis with Triton X-100 (TTX). C) Membrane mixing during stirring in the spectrophotometer cuvette. The inset shows magnification of the initial kinetics. The amount of LUVs corresponds to 1.25 mg mL^{-1} amphiphile concentration, KCl is 250 mM.

To circumvent the unfavorable effect of DiR, we next employed two FRET pairs in a similar assay based on dilution. We first used NBD- and Rho-labeled 1,2-dipalmitoyl-sn-glycero-3-phosphoethanolamine (PE) and monitored the NBD emission upon its excitation (**Figure 3**A). Membrane mixing occurred fairly linearly and leveled off after about 2 h under agitation at 1200 rpm in the laboratory vortex mixer. We confirmed by a shorter experiment and lysis with Triton X-100 that at this point the arbitrary 100% (full FRET loss) was achieved (Figure 3B). Under the gentle stirring in the spectrophotometer, the fusion efficiency was lower as expected; in 20 h it barely exceeded 30% (Figure 3C). Under these conditions, we ascribed the initial transient response to vesicle docking and subsequent disaggregation, while steady membrane mixing initiated after 2 h. Micrographs of the resulting suspensions revealed homogeneous GUVs (Figure S17, Supporting Information), which indicated that 1.5 mol% labeled lipids did not suppress growth as did the 20 mol% DOPC in hybrids, while occasional brighter spots suggested aggregated LUVs or accumulation of tagged lipids.

Even though labeled lipids were a small fraction of the total amphiphiles and apparently did not affect growth, we repeated the experiment with labeled polymers, whereby the FRET donor was FTIC instead of NBD. In this scenario, we monitored acceptor emission upon donor excitation. Under the same salt and agitation conditions, the intermittently measured Rho fluorescence decreased to zero within about 20 min and the course was nearly identical in three samples (Figure S18, Supporting Information). In parallel, we checked the effect of the reporter dye and monitored the FITC excitation/emission under constant stirring in the spectrophotometer; the mixing efficiency was again lower, as expected (Figure S19, Supporting Information). Altogether, the variable courses in different assays suggest that an absolute kinetic quantification is virtually impossible and highly dependent on the chosen assay. Nevertheless, comparative analysis within the same setups clearly indicates that the vesicles undergo some form of fusion within the first minutes of agitation, before any detectable change in size distribution, and that milder stirring has a smaller effect than vortexing.

As shown in the previous section by DLS, the agitation at 1200 rpm in presence of NaCl and $MgCl_2$ simultaneously stimulated growth and fission. FRET data with labeled lipids demonstrated that all salts had a similar effect on the membrane mixing during stirring in the spectrophotometric cuvette but the process slowed down after about 5 h in the case of 250 mM NaCl and 125 mM $MgCl_2$ (Figure S20, Supporting Information). In both NaCl and $MgCl_2$ we did not find any visible structures when 1.25 mg mL^{-1} polymersomes were agitated for 24–48 h. Increasing the polymersome concentration to 5 mg mL^{-1} did not help to form GUVs after 48 h at 1200 rpm either. We rarely detected 1–3 μm multilamellar (Figure S21, Supporting Information) and

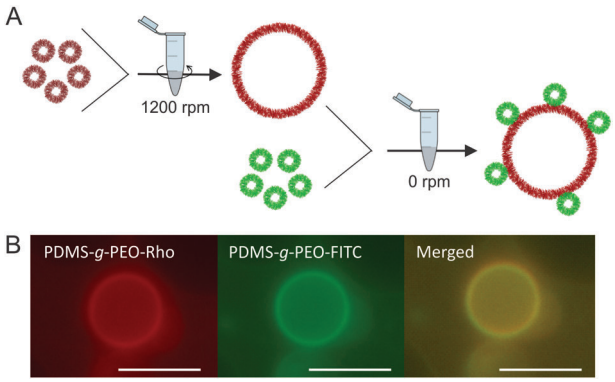

Figure 4. Mixing of PDMS-*g*-PEO LUVs and GUVs in 250 mM KCl. A) Schematic representation of the docking assay. B) Representative epifluorescence micrograph. LUVs are tagged with PDMS-*g*-PEO-FITC (green) and GUVs with PDMS-*g*-PEO-Rho (red). Scale bars: 5 µm.

larger multivesicular vesicles (Figures S22 and S23, Supporting Information), while the majority of the polymer constituted long multilamellar tubes (Figure S24, Supporting Information) and polymer beads (Figure S25, Supporting Information). Such an increase in lamellarity with increasing NaCl concentration was previously observed for DOPC vesicles[33] and multilamellar tubes were formed upon contact with water.[34]

2.3. Analysis of Individual Compartments

The current protocol resulted in multiple fusion events leading to a vesicle size increase of two orders of magnitude. To further analyze this process, we monitored LUVs docking on newly grown GUVs by tagging them with different dyes (LUVs with PDMS-*g*-PEO-FITC and GUVs with PDMS-*g*-PEO-Rho) (**Figure 4**A).

Indeed, the green signal of LUVs colocalized with the red membrane of preformed GUVs (Figure 4B) but its intensity varied (Figure S26, Supporting Information) likely due to varying LUV distribution within the sample (no extensive mixing was introduced in order not to break the GUVs, instead the Eppendorf tube was only gently tapped upon mixing of both suspensions).

In order to control the mass transport of the LUVs we next analyzed the docking process in a microfluidic setup with confocal microscopy.[35] To this end, we prepared polymer FTIC-tagged GUVs by electroformation in ≈500 mM sucrose, trapped them in the microfluidic chip, and introduced Rho-tagged LUVs in 250 mM KCl at a flow rate of 1 µL min^{-1} (**Figure 5**). Due to asymmetric ion distribution across the membrane, the GUVs exhibited tubulation[36] (see green signal inside the GUV image in Figure 5) and limited stability (Figure S27 and Video S1, Supporting Information). The latter, was slightly improved by coating the chip with BSA (bursting decreased). After 30 min of flushing, the Rho signal accumulated on the GUV membrane, which confirmed docking and possible hemifusion (Figure 5, see also Figures S28 and S29, Supporting Information).

2.4. Role of Salts in Polymersome Fusion

Unlike the more sophisticated orchestration of fusion by protein pores, the proximity model postulates that close apposition of membranes and small perturbations suffice to induce fusion. Although this mechanism has been developed for liposomes,[37] it was recently extended to the fusion of polymer vesicles,[20] and is likely valid for the current case. The strong agitation facilitates the contacts between PDMS-*g*-PEO polymersomes and destabilizes their membranes, whereby these effects could be possibly implemented by other mechanical means such as ultrasound treatment.[20] 1200 rpm appears to be a sweet spot between the sufficient agitation to ensure multiple vesicle collisions on the one side and the comparatively high shear stress in the vortex mixer, resulting in rupture and fission, on the other (we note that this vortex magnitude was identified from DLS experiments and the optimum may slightly deviate). However, aggregation and growth was not observed in the absence of salts at and beyond physiological levels[38] despite the fact that the zeta potential in Milli-Q water was close to zero (-2 ± 1 mV). In theory, values in this range suggest colloidal instability and the polymersomes would be expected to aggregate readily but the size distribution did not change in a week, as discussed above. On the other side, even if some charge was introduced to the membrane via the dyes, it was neutralized in the presence of salts (Figure S8, Supporting Information). However, we refrain from interpretation based on electrostatic interactions because of the low magnitude of the latter change and the potential inaccuracy arising from different ionic strengths and aggregation,[39] and the nearly neutral zeta potential in absence of salts.

The association between PEO chains and Mg^{2+} is expected to be even stronger than with Na^+ or K^+ due to the smaller ionic radius and higher electronegativity.[40] The effectiveness of salts, however, does not follow the ionic strength—equal salting-out power of K_2SO_4 and $MgSO_4$,[41] and KCl and NaCl[42] was previously observed. The salting-out effect reduces the steric resistance between vesicles[42] and enables docking, which is a prerequisite to fusion. We observed GUV clustering, as exemplified in Figures S4 and S6, Supporting Information, and discussed above.

The cations in this study can partition between four environments: 1) free in water, 2) bound to the chloride anions, 3) bound to the PEO oxygen atoms, or 4) bound to the lipid headgroup oxygen atoms in the case when lipids were used. Molecular dynamics simulations previously showed that Na^+ ions were predominately bound to PEO but also to a lesser degree to the lipid headgroup.[43] K^+ ions were also found in the PEO layer, though a larger portion of them remained in solution outside the membrane than in the case of Na^+ cations, which indicated weaker interaction. The rationale for the latter lies in the natural curvature of PEO chain that fits more comfortably around Na^+ than K^+ ions.[44] We speculate that under the present conditions, the stronger association led to fission events in addition to fusion, and formation of multilamellar tubes instead of spherical giant vesicles (Figure S25, Supporting Information).

Molecular dynamics simulations also showed that the thickness of the PEO layer was slightly expanded in the presence of salt, which can be explained by the greater number of bound cations, which increase the electrostatic repulsion within the layer.[43] To inspect if such changes in the hydrophilic portion of the polymer membrane cause changes in the overall packing, we analyzed the salt effect by the polarity-sensitive fluorescent probe Laurdan.[45] PDMS-*g*-PEO membranes exhibited similar disorder in Milli-Q water and in mono and divalent salt

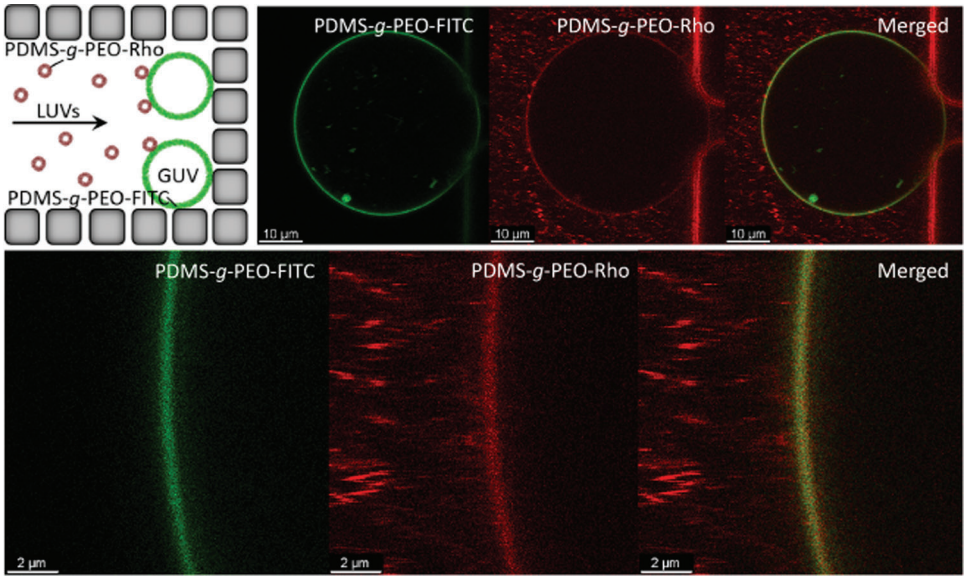

Figure 5. Membrane mixing experiment in microfluidics. GUVs are trapped in a microfluidic chip with multiple rectangular traps, similar to those in ref. [35], with a gap size of about 10 μm between the posts. GUVs prepared in ≈500 mM sucrose and labeled with PDMS-*g*-PEO-FITC (green) are exposed to a flow of LUVs, labeled with PDMS-*g*-PEO-Rho (red) in isosmotic 250 mM KCl.

solutions (Figure S30B, Supporting Information), thus the PDMS phase apparently remained unaltered. Meanwhile, we previously observed that salt had an effect on membrane bending rigidity: even 5 mM KCl softened PDMS-*g*-PEO membranes (bending rigidity decreased from 11.7 $\kappa_B T$[14] to 6.1 $\kappa_B T$[16]), which in turn positively affected SNARE-mediated polymersome fusion. Similarly, a slight increase in salt concentration (from 0 to ≈50 mM) was shown to decrease the bending rigidity of fluid charged lipid membranes (POPC:POPG 1:1) by around 30 $k_B T$.[46] Furthermore, the combined effect of NaCl and Tris buffer was stronger than their individual contributions, giving rise to 40% reduction in bending rigidity of POPC GUVs.[47] On the other side, small-angle X-ray scattering evidenced that the bilayer thickness of zwitterionic DOPC vesicles increased in presence of NaCl.[33] In regard to the present case, we recently observed increase in the membrane thickness of PDMS-*g*-PEO/phosphatidylcholine (70:30 molar ratio) mixtures in presence of KCl via cryo electron microscopy: in absence of salt the thickness was 4.9 nm,[14] while in buffer containing 150 mM KCl it was 6.1 nm.[16] Thus, the fusion in the present case is attributed to PEO expansion upon interaction with salts, contrary to the previously assumed corona contraction in the case of PBd-*b*-PEO,[23] which expansion in turn softens the membrane and thus lowers the energetic barriers during fusion-related deformations. Similar effect of the size of the headgroup on the bending rigidity was observed via simulations in the case of phospholipids.[48]

2.5. Compatibility of the Protocol with Essential Artificial Cell Features

Finally, we investigated whether this simple procedure to grow optically accessible polymer compartments can be integrated with the encapsulation of cytosolic components and the reconstitution of membrane machinery. This practical rationale lines with the reductionist view of the cell as a functionalized, closed membrane, which accommodates water-soluble machinery and metabolites in its lumen. We approached this by introducing different hydrophilic molecules (at 10 μM final concentration) to the LUVs in 250 mM KCl, and after 24 h of agitation at 1200 rpm, we analyzed their partitioning via fluorescence microscopy (**Figure 6**A). First, we tested calcein—a small fluorescent dye (MW = 623 g mol^{-1}), which is commonly used to monitor vesicle leakage and content mixing during fusion. The size of the GUVs was overall smaller than in the absence of the dye but calcein was distributed fairly homogenously (Figure 6B and Figure S31, Supporting Information). To test if larger molecules also entered the polymersomes, we next employed FITC-labeled dextran (MW = 20 000 g mol^{-1}). The resulting varying distribution was likely a result from the stochasticity of the growth process and the slower dextran mass transport (Figure 6C and Figures S32 and S33, Supporting Information). Finally, we added a model nucleotide (FITC-12-dUTP) to probe the encapsulation of information carriers. Interestingly, when we agitated LUVs in presence of FITC-12-dUTP, much larger GUVs were formed (reaching diameters of ≈50 μm). We assume that growth was facilitated by FITC-12-dUTP due to stronger attractive forces between the vesicles. This could be explained by K^+ bridging between PEO and the phosphate group of dUTP since it was shown that ATP associates with DOPC bilayers.[49] These membrane interactions led to heterogeneous distribution of FITC-12-d-UTP (Figure 6D and Figures S34 and S35, Supporting Information) and often resulted in tight contacts between the GUVs and formation of tissue-like structure (Figure S36, Supporting Information).

The harsh agitation may in parallel turn harmful to sensitive membrane proteins due to, for example, membrane destabilization and subsequent protein delipidation. To test for such a potential detrimental effect, we reconstituted the 144 kDa,

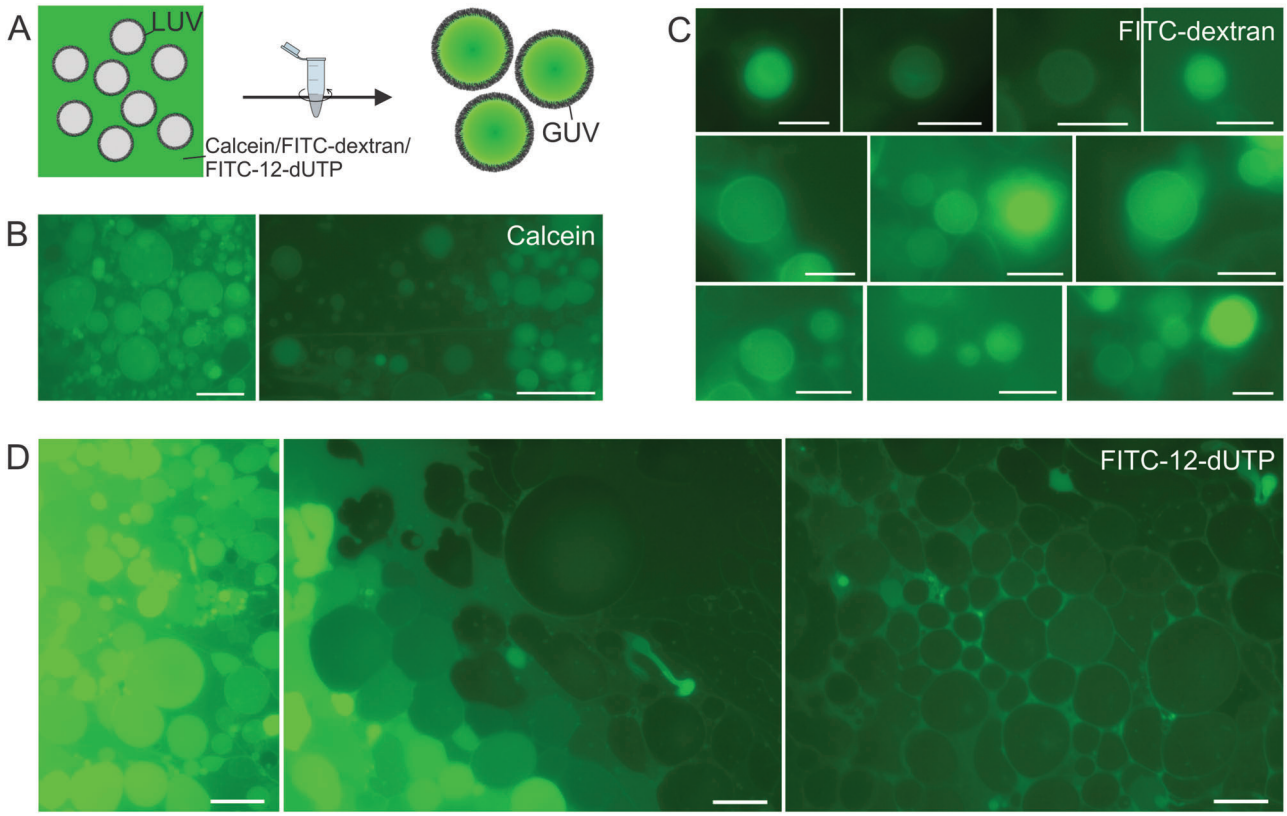

Figure 6. Uptake of cytosolic load during growth of GUVs from LUVs. A) Scheme representing the encapsulation experiment. Representative micrographs of PDMS-*g*-PEO GUVs with encapsulated B) calcein. Scale bars: 10 µm. C) FITC-dextran. Scale bars: 5 µm. D) FITC-12-dUTP. Scale bars: 10 µm.

four-subunit bacterial proton pump ubiquinol bo_3 oxidase[50] in polymer LUVs and measured its enzymatic activity via oxygen consumption upon agitation at 1200 rpm. The latter enzyme has been extensively investigated alone[51] or integrated with other respiratory enzymes in minimal oxidative phosphorylation architectures.[24,52] Since we had observed that the activity of bo_3 oxidase dropped even at 4 °C (≈30% decrease after one day[14]), we also tested the behavior at room temperature. As a negative control, aggregated bo_3 oxidase was obtained by removing the stabilizing detergent (*n*-dodecyl *β*-D-maltoside) via Bio-Beads to mimic the detrimental influence of delipidation (**Figure 7**A). In parallel, we tested whether protein-functionalized membranes were still prone to fusion. Up to 4 h after reconstitution, we did not measure a decrease in protein activity at room temperature, regardless if the sample was agitated or not (Figure S37, Supporting Information), which gives a reasonable time window for experimentation. No difference was observed also between the activity at room temperature and at 4 °C either (Figure 7B). Furthermore, the size of the polymersomes with reconstituted protein increased (Figure 7C), which indicated that the protocol was compatible with this sensitive protein.

3. Conclusions

The favorable mechanical properties of PDMS-*g*-PEO enabled mimicking different cellular phenomena and architectures via simple experimental procedure and can be discussed in various biomimetic contexts—from parallels to the historical studies on Ca^{2+}-induced fusion of anionic liposomes[53] to reductionist synthetic biology scenarios for cellular growth and tissue formation. Here, unlike the natural process of sophisticated orchestration by proteins, fusion of said polymersomes was facilitated merely by the synergistic effect of salts for membrane expansion/softening and mechanical stress. The magnitude of the latter cue places the system outside the textbook notion of a classical secretory pathway with freely diffusing vesicles and reminisces an apposition mechanism for membrane exchange, conceptually similar to dough kneading. This in turn enabled cytosolic encapsulation during the formation of micrometer compartments, whereas a model membrane protein also survived the harsh agitation, indicating that artificial cells based on PDMS-*g*-PEO can be equipped with multiple cellular features via this straightforward method. Thus, the adoption of the previously reported protocol for PBd-*b*-PEO[23] and its optimization toward the current polymer enabled tight experimental control over the GUV quality and yield—an ample amount of large GUVs was reproducibly obtained only with particular KCl concentration and magnitude of agitation. Thereby, we followed the process at different length and time scales by light scattering, microscopy and FRET-based membrane mixing assays, and discussed the goldilocks effect of KCl. Altogether, the lamellar and size variability of GUV prepared by the current approach is comparable to conventional electroformation. However, it necessitates only the use of an extruder and a vortex mixer. To summarize, we found optimal parameters for

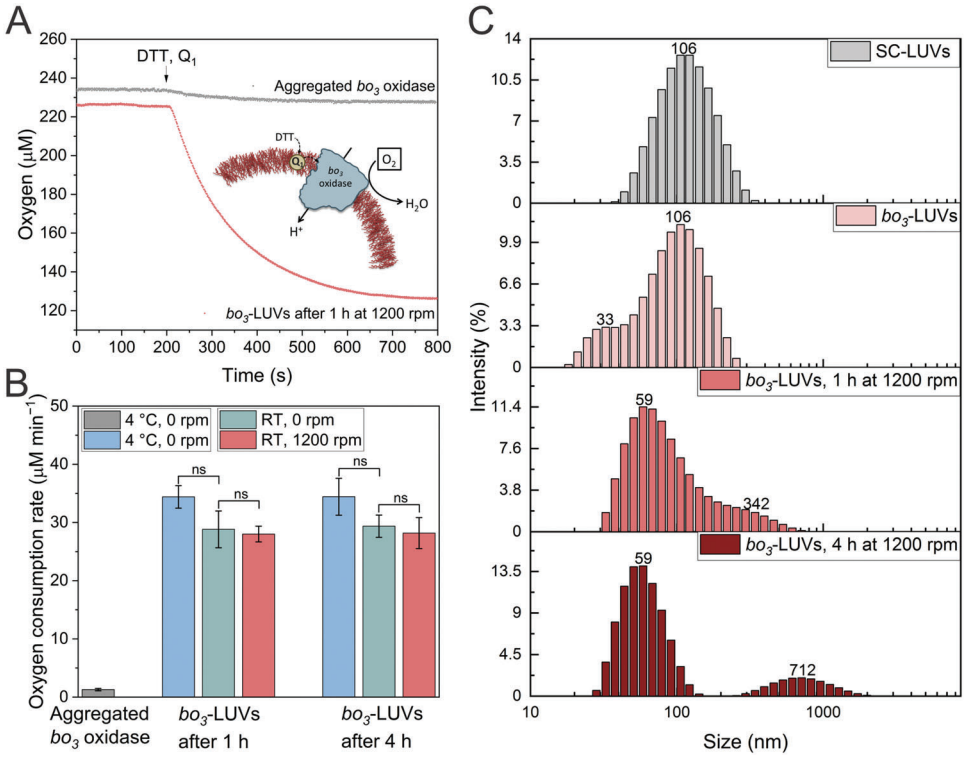

Figure 7. Activity and size distribution of bo_3-LUVs. A) Oxygen consumption by bo_3 oxidase reconstituted in PDMS-*g*-PEO LUVs and aggregated bo_3 oxidase (negative control in absence of stabilizing amphiphiles (detergent/polymer)). At ≈200 s mark, the enzyme reaction is initiated by dithiothreitol (DTT) and ubiquinol 1 (Q_1). B) Oxygen consumption rates by aggregated ($n = 2$) and reconstituted bo_3 oxidase ($n = 3$) upon incubation at 4 °C or room temperature (RT) in absence (0 rpm) and presence of agitation (1200 rpm). Statistical hypothesis test (Student's *t*-test) was applied, according to which the difference between two samples is not significant (ns) for a *p*-value > 0.05. C) Size distribution of LUVs with sodium cholate (SC) and bo_3-LUVs before and after agitation.

the uncomplicated growth of PDMS-*g*-PEO GUVs, whose properties potentially allow for reconstitution of various biomimetic features, beyond proton pumping or growth, while the facile compartmentalization should aid bottom-up synthetic biology studies at the scales of individual compartments and tissues.

4. Experimental Section

Chemicals: 1,2-dioleoyl-sn-glycero-3-phosphocholine (DOPC), 1,2-dipalmitoyl-sn-glycero-3-phosphoethanolamine-*N*-(7-nitro-2-1,3-benzoxadiazol-4-yl) (ammonium salt) (PE-NBD) and 1,2-dioleoyl-sn-glycero-3-phosphoethanolamine-*N*-(lissamine rhodamine B sulfonyl) (PE-Rho) were purchased from Avanti Polar Lipids. NHS-rhodamine, NHS-fluorescein, sulforhodamin B, calcein and 1,1″-dioctadecyl-3,3,3″,3′-tetramethylindotricarbocyanine iodide (DiR) were purchased from Thermo Fisher Scientific. Fluorescein isothiocyanate-dextran (FITC-dextran; MW 20 000 g mol^{-1}) and fluorescein-12-dUTP (FITC-12-dUTP) were purchased from Merck. PDMS-*g*-PEO was a kind gift from Dow Corning. The viscosity-average molecular weight of 3000 g mol^{-1}, the 47% weight fraction of ethylene oxide (2 arms of PEO per PDMS chain, on average) and the average degree of side chain polymerization of 12 and main chain polymerization of 26 were reported in the data sheet provided by the supplier. PDMS-*g*-PEO labeled with fluorescein (PDMS-g-PEO-FITC) or rhodamine (PDMS-*g*-PEO-Rho) was synthesized following a previously described procedure.[26]

Preparation of LUVs for Bulk Growth Experiments: Liposomes were prepared from DOPC, hybrids from PDMS-*g*-PEO:DOPC (80:20, mol/mol) and polymersomes from PDMS-*g*-PEO. 5 mg of lipid, lipid/polymer mixture or polymer in chloroform:methanol (2:1, v/v) were deposited in a glass vial and the solvent was removed by evaporation under a gentle stream of nitrogen for ≈30 min. The thin lipid, lipid/polymer or polymer film was rehydrated with salt solution, Milli-Q water or sucrose solution and re-suspended at a final lipid concentration of 5 mg mL^{-1} by vortexing. The resulting suspension of multilamellar vesicles (MLVs) was subjected to five freeze-thaw cycles (1 min liquid nitrogen, then water bath at 35 °C until thawed completely, followed by 30 s vortexing). The freeze-thaw step was skipped for polymersomes. Finally, the size and lamellarity of vesicles in the suspension was unified by extrusion (11 times) through polycarbonate membrane with a pore size of 200 nm in Mini Extruder.

Size Distribution via Dynamic Light Scattering: Size and dispersity of LUVs was determined by dynamic light scattering (DLS). DLS experiments were performed using a Zetasizer Nano ZS (Malvern, Worcestershire, UK) with a 633 nm helium-neon laser with back-scattering detection. The vesicle suspensions (1.25 mg mL^{-1}) before and after agitation were measured at a fixed 173° scattering angle in 45-μL quartz cuvette (3 mm light path).

Determination of Zeta Potential: Zeta potential measurements were done with Zetasizer Nano ZS (Malvern, Worcestershire, UK). 1 mL of Milli-Q or salt solution (250 mM KCl, 250 mM NaCl or 125 mM $MgCl_2$) was transferred with glass syringe into disposable folded capillary cell DTS 1070. Next, ≈100 μL of polymersome suspension (60 mg mL^{-1}) was transferred to the bottom of the cell and the zeta potential was measured directly after that. Zeta potential was measured with the following settings: model Smoluchowski, 23 °C, equilibration time 0 s, data processing monomodal analysis, number of measurements 1, runs 10–400. Each sample was measured 7–8 times.

GUV Analysis by Fluorescence Microscopy: Polymersomes, exposed to agitation in KCl solution, were evaluated for size, membrane dye distribution and structural integrity by fluorescence microscope Axio Imager.M1 (Zeiss) with 100× oil objective (NA 1.3) in Axio Vision Rel. 4.8 software. To visualize membrane dyes and encapsulated molecules, rhodamine and FITC filter sets were used. To decrease vesicle rupture, poly(lysine)-coated glass slides were used.

Membrane Mixing Analysis by Fluorescence Resonance Energy Transfer: Tagged polymersomes for membrane mixing analysis by fluorescence resonance energy transfer (FRET) measurements contained 0.6 mol% of PDMS-*g*-PEO-Rho and 0.6 mol% PDMS-*g*-PEO-FITC or 1.5 mol% PE-Rho and 1.5 mol% PE-NBD. Fluorescence was monitored via excitation and emission of FITC or NBD (460/535 nm; 5/10 nm, 0.1 s) in a fluorescence spectrophotometer Cary Eclipse. To this end, 937.5 µL of 250 mM KCl was transferred in a quartz cuvette and blank/reference (zero) was measured. Next, 12.5 µL of tagged polymersomes (20 mg mL^{-1}) were added and the baseline was monitored while stirring. To dilute the tagged polymersomes, 50 µL of dye-free polymersomes (20 mg mL^{-1}) were added and FRET was monitored for ≈20 h while stirring. To obtain total dequenching, vesicles were lysed by adding 10% Triton X-100 (TTX) in 10 µL aliquots until reaching maximal fluorescence.

Analysis of GUV-LUV Docking in Bulk: PDMS-*g*-PEO GUVs were grown by agitation (1200 rpm) of PDMS-*g*-PEO LUVs (5 mg mL^{-1}) tagged with 0.6 mol% PDMS-*g*-PEO-Rho. PDMS-*g*-PEO LUVs, tagged with 0.6 mol% PDMS-*g*-PEO-FITC were added to GUVs (final concentration of LUVs was 1 mg mL^{-1}) and incubated for 5 min at room temperature in absence of agitation. Docking was analyzed directly after incubation via fluorescence microscopy.

Wafer Design and Fabrication: The wafer was designed and fabricated as described previously.[14,54]

Chip Fabrication: Microfluidic chips were produced as described previously.[14,54] Each post in the trap had a dimension of 40 µm × 40 µm, and a height of ≈70 µm; the gap distance between two posts was 10 µm.

Chip Coating: The microchannels of the device were filled with 2% (w/v) bovine serum albumin (BSA) solution by centrifugation and incubated for 30 min at room temperature to prevent GUV surface adhesion and rupture. After incubation, BSA solution was replaced with 100 µL of ≈500 mM sucrose using a syringe pump in withdraw mode at 10 µL min^{-1}.

Preparation of GUVs by Electroformation: Polymer GUVs were prepared using the electroformation method. Briefly, ≈5 µL polymer solution (3.3 mM) was spread onto the conducting side of two ITO glasses and dried under vacuum for 2 h. The ITO glasses were assembled into a chamber with one Teflon spacer and the corresponding solution was introduced. An alternating electric field of 3.0 Vpp and 10 Hz was applied using a function generator for a period of 2 h. Then the GUVs were collected and used immediately.

GUVs Trapping and Monitoring of Potential Fusion Event: PDMS-*g*-PEO GUVs, tagged with PDMS-*g*-PEO-FITC, prepared in ≈500 mM sucrose were trapped in the microfluidic device. Next, 200 nm polymersomes, tagged with PDMS-*g*-PEO-Rho, prepared in isosmotic 250 mM KCl were flushed into the chip.

Encapsulation of Cytosolic Solutes: To PDMS-*g*-PEO LUVs (5 mg mL^{-1}), tagged with 0.6 mol% PDMS-*g*-PEO-Rho, calcein/FITC-dextran/FITC-12-dUTP were added at a final concentration of 10 µM each, and agitated at 1200 rpm for 24 h. Encapsulation efficiency was qualitatively analyzed by fluorescence microscopy.

Reconstitution of bo_3 Oxidase in LUVs: bo_3 oxidase was reconstituted in polymersomes (extruded through 200 nm-pore size membrane) via the authors' previous protocol[24] with slight modifications, at polymer to protein molar ratio of 9000:1. Shortly, to 20 mg mL^{-1} polymersomes prepared with 0.4% sodium cholate (in 1 mM Tris-HCl (pH 7.5), 250 mM KCl), bo_3 oxidase was added at a final concentration of 0.74 µM, and incubated for 30 min at 4 °C. Detergent was removed by addition of Bio-Beads in three 30-min steps (90 mg for 200 µL of reconstitution mixture).

Aggregated bo_3 Oxidase: To obtain aggregated bo_3 oxidase, all the steps were repeated as for reconstitution, with the exception that the vesicle suspension was replaced by buffer (1 mM Tris-HCl (pH 7.5), 250 mM KCl).

Oxygen Consumption Measurements: The activity of bo_3-LUVs and aggregated bo_3 oxidase was determined via oxygen consumption with an Oxytherm system (Hansatech Instruments). Steady-state activity of reconstituted bo_3 oxidase was determined as described by,[24,52b] with slight modifications. The samples were measured directly after reconstitution and after agitation at 1200 rpm at different time points. Briefly, 14 µL bo_3-LUVs were mixed with 210 µL buffer (1 mM Tris-HCl (pH 7.5), 250 mM KCl) in 1.5-mL Eppendorf tube to obtain final polymersome concentration of 1.25 mg mL^{-1}. Next, diluted bo_3-LUVs were agitated for 1 or 3 h at 1200 rpm at room temperature, and protein activity was measured directly after that. The total measurement volume in Oxytherm was 500 µL and the final bo_3 oxidase concentration was ≈20.7 nM. bo_3 oxidase was activated by addition of dithiothreitol (DTT, at a final concentration of 8 mM) and ubiquinol 1 (Q_1 at a final concentration of 40 µM). The oxygen consumption rates were reported as the average of 2–3 measurements, with standard deviation. All measurements were done at 22 °C while stirring.

Supporting Information

Supporting Information is available from the Wiley Online Library or from the author.

Acknowledgements

This work was part of the MaxSynBio consortium which is jointly funded by the Federal Ministry of Education and Research (BMBF) of Germany and the Max Planck Society. This research was supported by the EU-program ERDF (European Regional Development Fund) of the German Federal State Saxony-Anhalt within the Research Center of Dynamic Systems (CDS). The authors are grateful to Anne Christin Reichelt and Sarah Reichstetter for their help with DLS measurements, to Claudia Bednarz for isolation and purification of bo_3 oxidase, and to the group of Dr. Steffen Klamt (Analysis and Redesign of Biological Networks) for allowing access to their fluorescence microscope and fluorescence spectrophotometer.

Open access funding enabled and organized by Projekt DEAL.

Conflict of Interest

The authors declare no conflict of interest.

Data Availability Statement

The data that support the findings of this study are available in the supplementary material of this article.

Keywords

biomimetics, fusion, microfluidics, polymersomes, vesicles

Received: November 3, 2021
Published online: December 5, 2021

[1] P. Schwille, J. Spatz, K. Landfester, E. Bodenschatz, S. Herminghaus, V. Sourjik, T. J. Erb, P. Bastiaens, R. Lipowsky, A. Hyman, P. Dabrock, J.-C. Baret, T. Vidakovic-Koch, P. Bieling, R. Dimova, H. Mutschler, T. Robinson, T.-Y. D. Tang, S. Wegner, K. Sundmacher, *Angew. Chem., Int. Ed.* **2018**, *57*, 13382.
[2] T. Gánti, *Biosystems* **1975**, *7*, 15.
[3] M. Exterkate, A. Caforio, M. C. A. Stuart, A. J. M. Driessen, *ACS Synth. Biol.* **2018**, *7*, 153.

[4] D. Blanken, D. Foschepoth, A. C. Serrão, C. Danelon, *Nat. Commun.* **2020**, *11*, 4317.
[5] G. Van Meer, D. R. Voelker, G. W. Feigenson, *Nat. Rev. Mol. Cell Biol.* **2008**, *9*, 112.
[6] D. R. Voelker, *Trends Biochem. Sci.* **2005**, *30*, 396.
[7] E. Quon, Y. Y. Sere, N. Chauhan, J. Johansen, D. P. Sullivan, J. S. Dittman, W. J. Rice, R. B. Chan, G. Di Paolo, C. T. Beh, A. K. Menon, *PLoS Biol.* **2018**, *16*, e2003864.
[8] I. Ivanov, R. B. Lira, T.-Y. D. Tang, T. Franzmann, A. Klosin, L. C. Da Silva, A. Hyman, K. Landfester, R. Lipowsky, K. Sundmacher, R. Dimova, *Adv. Biosyst.* **2019**, *3*, 1800314.
[9] R. B. Lira, T. Robinson, R. Dimova, K. A. Riske, *Biophys. J.* **2019**, *116*, 79.
[10] S. Deshpande, S. Wunnava, D. Hueting, C. Dekker, *Small* **2019**, *15*, 1902898.
[11] E. Rideau, R. Dimova, P. Schwille, F. R. Wurm, K. Landfester, *Chem. Soc. Rev.* **2018**, *47*, 8572.
[12] B. M. Discher, Y.-Y. Won, D. S. Ege, J. C.-M. Lee, F. S. Bates, D. E. Discher, D. A. Hammer, *Science* **1999**, *284*, 1143.
[13] a) S. Khan, M. Li, S. P. Muench, L. J. Jeuken, P. A. Beales, *Chem. Commun.* **2016**, *52*, 11020; b) C. Kleineberg, C. Wölfer, A. Abbasnia, D. Pischel, C. Bednarz, I. Ivanov, T. Heitkamp, M. Börsch, K. Sundmacher, T. Vidaković-Koch, *ChemBioChem* **2020**, *21*, 2149.
[14] N. Marušič, L. Otrin, Z. Zhao, R. B. Lira, F. L. Kyrilis, F. Hamdi, P. L. Kastritis, T. Vidaković-Koch, I. Ivanov, K. Sundmacher, R. Dimova, *Proc. Natl. Acad. Sci. USA* **2020**, *117*, 15006.
[15] R. S. M. Rikken, H. Engelkamp, R. J. M. Nolte, J. C. Maan, J. C. M. Van Hest, D. A. Wilson, P. C. M. Christianen, *Nat. Commun.* **2016**, *7*, 12606.
[16] L. Otrin, A. Witkowska, N. Marušič, Z. Zhao, R. B. Lira, F. L. Kyrilis, F. Hamdi, I. Ivanov, R. Lipowsky, P. L. Kastritis, R. Dimova, K. Sundmacher, R. Jahn, T. Vidaković-Koch, *Nat. Commun.* **2021**, *12*, 4972.
[17] C. Sanson, J.-F. Le Meins, C. Schatz, A. Soum, S. Lecommandoux, *Soft Matter* **2010**, *6*, 1722.
[18] T. Litschel, K. A. Ganzinger, T. Movinkel, M. Heymann, T. Robinson, H. Mutschler, P. Schwille, *New J. Phys.* **2018**, *20*, 055008.
[19] W. Su, Y. Luo, Q. Yan, S.i Wu, K. Han, Q. Zhang, Y. Gu, Y. Li, *Macromol. Rapid Commun.* **2007**, *28*, 1251.
[20] Y. Zhou, D. Yan, *J. Am. Chem. Soc.* **2005**, *127*, 10468.
[21] S. Varlas, R. Keogh, Y. Xie, S. L. Horswell, J. C. Foster, R. K. O'reilly, *J. Am. Chem. Soc.* **2019**, *141*, 20234.
[22] T. P. Smart, C. Fernyhough, A. J. Ryan, G. Battaglia, *Macromol. Rapid Commun.* **2008**, *29*, 1855.
[23] I. M. Henderson, W. F. Paxton, *Angew. Chem., Int. Ed.* **2014**, *53*, 3372.
[24] L. Otrin, N. Marušič, C. Bednarz, T. Vidaković-Koch, I. Lieberwirth, K. Landfester, K. Sundmacher, *Nano Lett.* **2017**, *17*, 6816.
[25] I. M. Henderson, W. F. Paxton, *J. Polym. Sci., Part B: Polym. Phys.* **2015**, *53*, 297.
[26] M. Chemin, P.-M. Brun, S. Lecommandoux, O. Sandre, J.-F. Le Meins, *Soft Matter* **2012**, *8*, 2867.
[27] a) D. J. Woodbury, J. E. Hall, *Biophys. J.* **1988**, *54*, 1053; b) A. Finkelstein, J. Zimmerberg, F. S. Cohen, *Annu. Rev. Physiol.* **1986**, *48*, 163.
[28] A. Peyret, E. Ibarboure, A. Tron, L. Beauté, R. Rust, O. Sandre, N. D. Mcclenaghan, S. Lecommandoux, *Angew. Chem., Int. Ed.* **2017**, *56*, 1566.
[29] A. Carlsen, N. Glaser, J.-F. Le Meins, S. Lecommandoux, *Langmuir* **2011**, *27*, 4884.
[30] O. Biner, T. Schick, Y. Müller, C. Von Ballmoos, *FEBS Lett.* **2016**, *590*, 2051.
[31] I. M. Henderson, A. M. Collins, H. A. Quintana, G. A. Montaño, J. A. Martinez, W. F. Paxton, *Polymer* **2016**, *83*, 239.
[32] C. Kleusch, N. Hersch, B. Hoffmann, R. Merkel, A. Csiszár, *Molecules* **2012**, *17*, 1055.
[33] J. U. De Mel, S. Gupta, R. M. Perera, L.y Ngo, P. Zolnierczuk, M. Bleuel, S. V. Pingali, G. J. Schneider, *Langmuir* **2020**, *36*, 9356.
[34] T. Bhatia, *J. Colloid Interface Sci.* **2021**, *584*, 706.
[35] N. Yandrapalli, T. Robinson, *Lab Chip* **2019**, 626.
[36] M. Karimi, J. Steinkühler, D. Roy, R. Dasgupta, R. Lipowsky, R. Dimova, *Nano Lett.* **2018**, *18*, 7816.
[37] S. Martens, H. T. Mcmahon, *Nat. Rev. Mol. Cell Biol.* **2008**, *9*, 543.
[38] a) R. D. Moore, G. A. Morrill, *Biophys. J.* **1976**, *16*, 527; b) H. Naora, H. Naora, M. Izawa, V. G. Allfrey, A. E. Mirsky, *Proc. Natl. Acad. Sci. USA* **1962**, *48*, 853; c) A. M. P. Romani, *Arch. Biochem. Biophys.* **2011**, *512*, 1.
[39] G. V. Lowry, R. J. Hill, S. Harper, A. F. Rawle, C. O. Hendren, F. Klaessig, U. Nobbmann, P. Sayre, J. Rumble, *Environ. Sci. Nano* **2016**, *3*, 953.
[40] J. C. Lutter, T.-Y.u Wu, Y. Zhang, *J. Phys. Chem. B* **2013**, *117*, 10132.
[41] F. E. Bailey Jr, R. W. Callard, *J. Appl. Polym. Sci.* **1959**, *1*, 56.
[42] K. Yu, A. Eisenberg, *Macromolecules* **1998**, *31*, 3509.
[43] A. Magarkar, E. Karakas, M. Stepniewski, T. Róg, A. Bunker, *J. Phys. Chem. B* **2012**, *116*, 4212.
[44] P. Johansson, S. P. Gejji, J. Tegenfeldt, J. Lindgren, *Solid State Ion* **1996**, *86–88*, 297.
[45] L. A. Bagatolli, *Biochim. Biophys. Acta, Biomembr.* **2006**, *1758*, 1541.
[46] H. A. Faizi, S. L. Frey, J. Steinkühler, R. Dimova, P. M. Vlahovska, *Soft Matter* **2019**, *15*, 6006.
[47] H. Bouvrais, L. Duelund, J. H. Ipsen, *Langmuir* **2014**, *30*, 13.
[48] A. Sreekumari, R. Lipowsky, *J. Chem. Phys.* **2018**, *149*, 084901.
[49] A. Garcia, S. Pochinda, P. N. Elgaard-Jørgensen, H. Khandelia, R. J. Clarke, *Langmuir* **2019**, *35*, 9944.
[50] A. Musatov, J. Ortega-Lopez, B. Demeler, J. P. Osborne, R. B. Gennis, N. C. Robinson, *FEBS Lett.* **1999**, *457*, 153.
[51] a) M. Li, S. Khan, H. Rong, R. Tuma, N. S. Hatzakis, L. J. C. Jeuken, *Biochim. Biophys. Acta, Bioenerg.* **2017**, *1858*, 763; b) M. Li, S. K. Jørgensen, D. G. G. Mcmillan, Ł. Krzemiński, N. N. Daskalakis, R. H. Partanen, M. Tutkus, R. Tuma, D. Stamou, N. S. Hatzakis, L. J. C. Jeuken, *J. Am. Chem. Soc.* **2015**, *137*, 16055; c) J. Berg, S. Block, F. Höök, P. Brzezinski, *Isr. J. Chem.* **2017**, *57*, 437.
[52] a) C. Von Ballmoos, O. Biner, T. Nilsson, P. Brzezinski, *Biochim. Biophys. Acta* **2016**, *1857*, 321; b) T. Nilsson, C. R. Lundin, G. Nordlund, P. Ädelroth, C. Von Ballmoos, P. Brzezinski, *Sci. Rep.* **2016**, *6*, 24113; c) J. Sjöholm, J. Bergstrand, T. Nilsson, R. Šachl, C. V. Ballmoos, J. Widengren, P. Brzezinski, *Sci. Rep.* **2017**, *7*, 2926.
[53] a) J. Wilschut, N. Duzgunes, R. Fraley, D. Papahadjopoulos, *Biochemistry* **1980**, *19*, 6011; b) D. A. Kendall, R. C. Macdonald, *J. Biol. Chem.* **1982**, *257*, 13892.
[54] Z. Zhao, D. Roy, J. Steinkühler, T. Robinson, R. Lipowsky, R. Dimova, *Adv. Mater.* **2021**, https://doi.org/10.1002/adma.202106633.

